

# Multifold topological semimetals

Iñigo Robredo,<sup>1,2</sup> Niels Schröter,<sup>3</sup> Claudia Felser,<sup>1</sup> Jennifer Cano,<sup>4,5</sup> Barry Bradlyn,<sup>6</sup> and Maia G. Vergniory<sup>1,2</sup>

<sup>1</sup>Max Planck Institute for Chemical Physics of Solids, 01187, Dresden, Germany

<sup>2</sup>Donostia International Physics Center, 20018, Donostia - San Sebastian, Spain

<sup>3</sup>Max Planck Institut für Mikrostrukturphysik, 06120, Halle, Germany

<sup>4</sup>Department of Physics and Astronomy, Stony Brook University, 11794, Stony Brook, USA

<sup>5</sup>Center for Computational Quantum Physics, Flatiron Institute, 10010, New York, USA

<sup>6</sup>Department of Physics, University of Illinois, 61820, Urbana-Champaign, USA

The discovery of topological semimetals with multifold band crossings has opened up a new and exciting frontier in the field of topological physics. These materials exhibit large Chern numbers, leading to long double Fermi arcs on their surfaces, which are protected by either crystal symmetries or topological order. The impact of these multifold crossings extends beyond surface science, as they are not constrained by the Poincaré classification of quasiparticles and only need to respect the crystal symmetry of one of the 1651 magnetic space groups. Consequently, we observe the emergence of free fermionic excitations in solid-state systems that have no high-energy counterparts, protected by non-symmorphic symmetries. In this work, we review the recent theoretical and experimental progress made in the field of multifold topological semimetals. We begin with the theoretical prediction of the so-called multifold fermions and discuss the subsequent discoveries of chiral and magnetic topological semimetals. Several experiments that have realized chiral semimetals in spectroscopic measurements are described, and we discuss the future prospects of this field. These exciting developments have the potential to deepen our understanding of the fundamental properties of quantum matter and inspire new technological applications in the future.

## I. INTRODUCTION

The prediction of Dirac and Weyl fermions dates back to 1928 [1] and 1929 [2] respectively, when Dirac proposed a four-component wave function to describe massive spin-1/2 fermions and Weyl simplified it to a two-component spinor to describe massless particles. Despite decades of searching by particle physicists, Weyl fermions remained elusive for almost a century. However, in recent years, the search has shifted to condensed matter systems, where Weyl and Dirac fermions are observed as protected crossings in electronic Bloch bands near the Fermi level, in two (Dirac) and three dimensions (Dirac and Weyl). This shift in research has opened up new avenues for investigating the properties and applications of these exotic particles.

The first attempt to find a Dirac fermion in a solid state system was made in 1987, when Boyanovsky *et al.* [3] proposed PbTe as a platform to realize the parity anomaly of 2 + 1 dimensional QED, after the prediction of a Dirac crossing in its band structure. Unfortunately, the model was incomplete and the theoretical prediction proved incorrect [4]. A successful identification of a solid state Dirac fermion was delayed until many years later in graphene [5], a two-dimensional (2D) material consisting of a single layer of carbon atoms arranged in a hexagonal lattice. The two low-energy electronic bands in graphene are doubly degenerate and meet at two linearly dispersing crossing points, known as the Dirac cones or Dirac points because near these points electrons behave as massless Dirac fermions. Later, the 3D generalizations of graphene, known as Dirac semimetals, were predicted [6, 7] and observed [8, 9] in Cd<sub>3</sub>As<sub>2</sub> and Na<sub>3</sub>Bi.

It took longer to discover Weyl fermions in solid state

systems. The first prediction of the ubiquity of perturbatively stable, ungappable 2-fold crossings in noncentrosymmetric or non-TR-invariant crystals (Weyl nodes) was made by Herring in 1937 [10]. The first proposal on a realistic material, though, came much later. They were predicted in pyrochlore iridates [11, 12], which was followed by a roadmap to engineer Weyl fermions in topological insulator heterostructures [13]. Unlike Dirac fermions, Weyl fermions are unique to 3D systems, and they exhibit twofold band crossings near the Fermi level with linear dispersion in all three dimensions. They are protected by a topological invariant known as the Chern number, which allows them to appear at any point within the Brillouin zone (BZ). Soon after, the first manifestation of a Weyl node in a crystal was pointed out theoretically in HgCr<sub>2</sub>Se<sub>4</sub> by Wan *et al.* [14] and a Weyl node in Hg<sub>1-x-y</sub>Cd<sub>x</sub>Mn<sub>y</sub> by Bulmash *et al.* [15]. Unfortunately, none of these systems came to fruition experimentally. Weyl semimetals became finally a reality with the experimental discovery [16, 17] confirming the theoretically predicted [18, 19] Weyl nodes in the TaAs family of compounds. However, finding new materials exhibiting Weyl fermions remained a challenge.

A big step forward was taken when it was realized that the co-representations (coreps) of the little group [20] at the high-symmetry points in the BZ could correspond to nodal fermions [21, 22]. This discovery set the stage for the machinery to systematically identify new materials using first-principles calculations combined with crystal symmetry and group theory [23, 24]. In 2016 Bradlyn *et al.* [25] and Wieder *et al.* [26] recognized that non-symmorphic crystalline symmetries could stabilize previously undiscovered crossings with no analogs in high-energy physics. In these systems, the low-energy  $\mathbf{k} \cdot \mathbf{p}$

Hamiltonians do not resemble the dispersion relations of any relativistic particle. Yet, they exhibit an isotropic limit resembling a Weyl fermion,  $H = \mathbf{k} \cdot \mathbf{S}$ , with  $S_i$  a set of  $n$ -dimensional spin matrices. Initially dubbed the multifold fermions, these excitations introduced the field of multifold topological semimetals. The newly introduced band crossings can be 3-, 4-, 6- and 8-fold degenerate at the crossing point, which may or may not exhibit a topological charge depending on their crystal symmetry. In current parlance, these  $n$ -dimensional fermions are referred to as  $n$ -folds, with  $n$  denoting the dimension of the band crossing, which is the notation we will use throughout this work. This work reviews the classification of these  $n$ -fold fermions, along with recent theoretical and experimental advances.

The manuscript is organized in the following way: in Section II we will give a full classification of high-order crossings in the 1651 Shubnikov groups and provide a general procedure to identify these nodes in materials. Section III will review the recent progress in materials realization with particular focus in *chiral* crystals. In Section IV we provide the computational details of the band structure calculations in Section III. We conclude the manuscript with a discussion of future perspectives.

## II. CLASSIFICATION OF ALL SHUBNIKOV GROUPS AND GENERAL PROCEDURE

In this section, we classify the symmetry-protected nodal points that can exist at high symmetry points within magnetic space groups by first reviewing the Shubnikov groups that describe crystalline materials and then discussing the dimensionality of their coreps.

### A. Magnetic Space Group Types

Multifold fermions, unlike Weyl fermions, need symmetry protection to be stabilised. In a particular symmetry group, the symmetry operations and their commutation relations dictate the multifold fermions that the group can protect. We thus start by reviewing the classification of Shubnikov groups, which will serve as a basis for the classification of multifold fermions in crystalline materials.

There are 1651 Shubnikov groups, also named magnetic space groups (MSG), which can be classified into four types. First, the type I groups are those that contain only unitary crystalline symmetries, i.e., no time reversal symmetry (TRS) or combinations of crystalline symmetries and TRS. There are 230 such groups. They can describe some materials with magnetic order, but only a reduced subset of all commensurate magnetic orderings. Nonetheless, the type I groups provide the underlying structure from which the remaining MSGs can be constructed. Starting from a type I MSG,  $H$ , adding TRS as a group element creates a type II MSG (non-magnetic,

often referred to as ‘gray’ groups),  $G = \{E, \mathcal{T}\} \times H = H \cup \mathcal{T}H$ , with  $\mathcal{T}$  the TRS operator. These groups describe non-magnetic crystals, such as the ones analysed in the topological quantum chemistry database [27–30]. The remaining two types (type III and IV), the so called black-white groups, deal with the combination of TRS and unitary symmetries and can describe the remaining commensurate magnetic orderings. These MSGs can be written as  $G = H \cup \mathcal{T}g_0H$ , with  $H$  a type I MSG and  $g_0 \notin H$  a unitary symmetry. In this context, type IV groups are those that contain fractional translations in  $g_0H$ , while type III MSGs do not.

This exhausts the classification of magnetic symmetry groups, which can be used to describe all commensurate magnetic orderings. A further sub-classification of MSGs is obtained by distinguishing between the presence or absence of improper symmetries, that is, symmetries with determinant  $-1$ . If a MSG does not contain elements such as rotoinversions or mirrors that reverse spatial orientation it is called a Sohnke MSG and it gives rise to a *structurally chiral* crystal, while if it contains inversion symmetry, rotoinversions or mirrors it is non-chiral. This distinction is relevant because *only Sohnke MSGs can host topologically charged multifold fermions*. In non-Sohnke MSGs, symmetry prevents a multifold fermion from carrying a topological charge.

We now turn to identifying the MSGs that can host  $n$ -fold crossings in the presence of spin-orbit coupling (SOC). The first step is to find the  $n$ -dimensional ( $n = 3, 4, 6, 8$ ) irreducible coreps of each of the 1651 MSGs: an irreducible corep corresponds to an  $n$ -dimensional symmetry enforced degeneracy. This search can now be easily carried out by using the Bilbao Crystallographic Server (BCS) [31–33]. Preliminary work on this classification was carried out by Bradlyn et al [34], Chang et al [35] and Wieder et al [26] for type II MSGs and generalized to all MSGs by Cano et al [36].

### B. Multifold Fermions

We start by analysing the 3-fold fermion, which was first predicted in the type I MSG  $I2_131'$  (199.13) [34] as the  $\mathbf{k} \cdot \mathbf{p}$  Hamiltonian in the vicinity of the  $P = (1/4, 1/4, 1/4)$  point. This turns out to be the most general 3-fold fermion, to which all 3-fold fermions in all MSGs are equivalent. The continuum Hamiltonian reads:

$$H_{3\text{-fold}}(\phi, \mathbf{k}) = \begin{pmatrix} 0 & e^{i\phi}k_x & e^{-i\phi}k_y \\ e^{-i\phi}k_x & 0 & e^{i\phi}k_z \\ e^{i\phi}k_y & e^{-i\phi}k_z & 0 \end{pmatrix}, \quad (1)$$

where  $\phi$  is a free parameter in the type II MSGs but can be symmetry-restricted in other MSGs. In the particular case of  $\phi = \pi/2$ , the Hamiltonian in Eq. 1 takes the familiar form  $H_{3\text{-fold}}(\pi/2, \mathbf{k}) = \mathbf{k} \cdot \mathbf{S}$ , with  $\mathbf{S}_{x,y,z}$  the generators of the spin  $s = 1$  representation of  $SU(2)$ . Notice

TABLE I. List of MSGs containing 3-fold, 6-fold and 8-fold fermions in systems with significant SOC. Each cell lists the MSG and the  $\mathbf{k}$ -point at which the multifold fermion resides.

	Type I	Type II	Type III	Type IV
3-fold	199.12, 214.67, 220.89 P 206.37, 230.145	199.13, 214.68, 220.90 P	214.69, 220.91, 230.148 P	
	198.9, 205.33, 212.59 R 213.63		212.61, 213.65 R	198.11, 212.62, 213.66 R
6-fold		206.37, 230.145 P 198.10, 205.34, 212.60, 213.64 R	206.39, 230.147, 230.149 P 205.35 R	205.36 R
		130.424, 135.484 A		125.374, 126.385, 129.420 A 131.445, 132.458, 136.504 A
8-fold		218.82, 222.99, 223.105 R 220.90, 230.146 H	222.102, 223.108 R 230.149 H	215.73, 221.97, 224.115 R

that it resembles the Weyl Hamiltonian,  $H_{\text{Weyl}} = \mathbf{k} \cdot \boldsymbol{\sigma}$  (with  $\boldsymbol{\sigma}$  the vector of Pauli matrices), which is the special case of  $s = 1/2$ . Hence the 3-fold fermions are referred to as spin-1 Weyl fermions. The  $H_{3\text{-fold}}$  Hamiltonian is gapped away from the degeneracy point, so the Chern number of each band can be computed by computing the Chern number of a sphere enclosing the degeneracy point. This calculation reveals that the Chern number is  $-2/+2$  for the lower/upper bands and 0 for the middle band (see Fig. 1a). Noticeably, the 3-folds in type IV MSGs have an additional symmetry generator  $g = \{E|\frac{1}{2}\frac{1}{2}\frac{1}{2}\} \circ \mathcal{T}$ , which forces  $\phi = \pi/2$ . This Hamiltonian, which can only be achieved by fine-tuning in type I/II/III MSGs, provides an ideal situation where the energy gap away from the degeneracy point is maximized, thus allowing maximum range for Fermi arcs [36]. In Table I we list all MSGs which can host 3-fold fermions in systems with significant SOC and at which high symmetry  $k$ -point.

The 6-fold fermions can be constructed by using the 3-fold fermion as a building block. There are two classes of 6-fold fermions depending on whether the MSG is chiral: double spin-1 fermions and spin-1 Diracs, respectively. In chiral type II MSGs, TRS pins two symmetry-related copies of the 3-fold fermion in the same  $k$ -point. The bands are gapped in generic directions away from the degeneracy point and the topological charge distribution can be seen in Fig. 1b. The two lower bands have topological charges of -2 each, while the middle ones have 0 charge, which amounts to a total of -4 at half-filling, the maximum topological charge of multifold fermions in the MSGs. In non-chiral type II MSGs, inversion (or rotoinversion) symmetry pins two 3-folds with opposite topological charge at the same  $k$ -point. In this case, the bands are doubly degenerate in generic directions away from the degeneracy point and the topological charge is 0 for all bands. These 6-folds are usually called spin-1 Dirac fermions, since the original Dirac fermion can be decomposed into two spin-1/2 Weyl fermions of opposite charge. In type III MSGs, all 6-folds are of spin-1 Dirac type, due to the presence of  $\mathcal{I} \circ \mathcal{T}$  symmetry. In type

IV MSG  $P1a\bar{3}$  (205.36), the 6-fold is also spin-1 Dirac, but the extra symmetries in the little co-group force the parameters to be pinned at an exactly solvable point in parameter space, similarly to what happens to the 3-folds in type IV MSGs.

It is natural to ask whether there are higher-dimensional effective Hamiltonians of the form  $H = \mathbf{k} \cdot \mathbf{S}$ . An exhaustive search of all MSGs revealed a 4-dimensional version of this Hamiltonian, usually referred to as a Rarita-Schwinger (RS) or spin-3/2 fermion, due to its analogy to high-energy physics[37] [36, 38, 39]. In this case, the  $S_{x,y,z}$  matrices are the generators of the spin  $s = 3/2$  representation (also denoted as  $S_{x,y,z}^{3/2}$ ) and the resulting Chern numbers of the bands are  $-3, -1, 1$  and  $3$ , respectively (see Fig. 1c). At half filling (two occupied bands) these quasiparticles have maximum topological charge,  $1 + 3 = 4$ . Noticeably, they can only be hosted in Sohnke MSGs, as rotoinversions pin two copies with opposite charge at the same point. In Ref. [34] the authors list the type II MSGs where these multifold fermions occur. However, there has been no extensive search for spin-3/2 multifold fermions in type III or type IV MSGs.

Analogous to the 3-fold, for certain material parameters the 4-fold Hamiltonian is adiabatically connected to the  $H_{3/2} = \mathbf{k} \cdot \mathbf{S}^{3/2}$  Hamiltonian described before, with Chern numbers  $-3, -1, 1, 3$ . This phase is realized in most known materials with fourfold fermions (see Sec. III). However, the 4-fold  $\mathbf{k} \cdot \mathbf{p}$  Hamiltonian also admits phases not adiabatically connected to  $H_{3/2}$  [34]. It was recently shown [40] that for certain parameter values the fourfold can exhibit Chern numbers  $-3, +5, -5, +3$  in the four bands. In the same work, they propose BaAsPt as a material displaying this phase of the 4-fold fermion. Finding experimental prove of a material that realizes this interesting phase is an active area of study.

Similar to how (spin-1/2 or spin-1) Dirac fermions can be decomposed into two (spin-1/2 or spin-1) Weyl fermions with opposite chirality, which are pinned to the same energy and momentum by symmetry, certain 8-fold

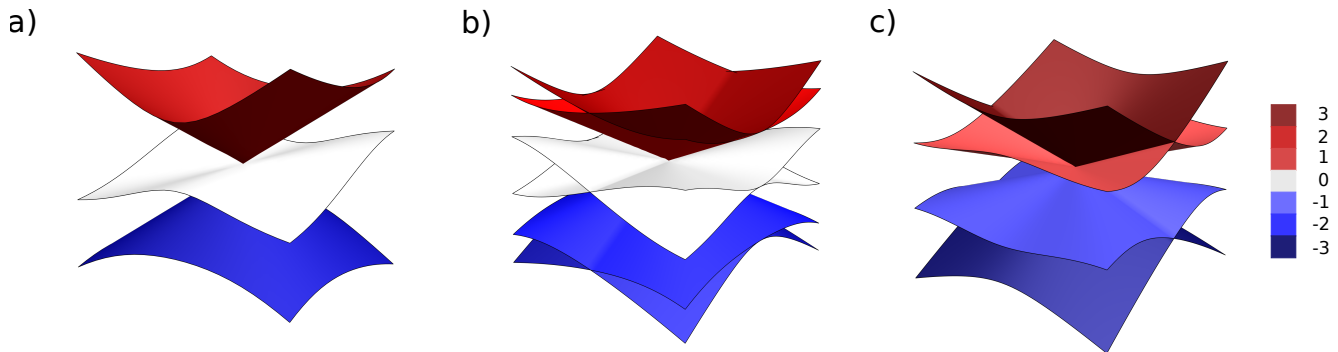


FIG. 1. Topologically charged multifold fermion dispersions. a) 3-fold spin-1, b) 6-fold double spin-1 and c) 4-fold RS fermion. The color code shows the topological charge (Chern number) of each band.

fermions can be decomposed into two copies of 4-folds. The 8-fold degeneracy is the highest possible in crystalline solids [41]. The 8-fold fermions hosted in cubic MSGs are formed by two spin-3/2 4-fold fermions with opposite charge that are pinned together by symmetry. The result is doubly degenerate bands in generic directions and no net topological charge.

The 8-fold fermions in the tetragonal MSGs, though, are fundamentally different. In that case, if inversion symmetry is removed as a group generator, a 4-dimensional corep yields a fermion isomorphic to a spin-1/2 Dirac. Inversion symmetry doubles this corep to create the 8-fold fermion. Thus, the tetragonal 8-fold can be thought of as a double spin-1/2 Dirac.

These two types of 8-fold fermions – the doubled spin-3/2 fermion and doubled spin-1/2 Dirac – are the only types of 8-fold fermions protected by crystalline symmetry. The two of them have in common that all bands are doubly degenerate in arbitrary directions from the node and have 0 topological charge.

We now turn to the type III and type IV MSGs. In type III MSGs the same results apply, since a type III MSG with an 8-fold degeneracy is a subgroup of a type II MSG with that same 8-fold degeneracy. In type IV MSGs, all 8-folds are of the double spin-1/2 Dirac form. However, similar to the 3-fold and 6-fold fermions in type IV MSGs, the little cogroup symmetries pin the Hamiltonian to a particularly simple form. In this case, the result is 8-fold fermions that are perfectly isotropic double spin-1/2 Dirac fermions. In Table I we show all MSGs that can host 8-fold fermions.

### III. MATERIAL REALIZATIONS

In this section we will describe the material realisations of the multifolds described in previous sections.

#### A. Non-magnetic materials

The theoretical prediction of multifold fermions led to a huge advance in material realisations, particularly in nonmagnetic systems. 3-fold fermions have been reported in chiral  $\text{Pd}_3\text{Bi}_2\text{S}_2$  in SG  $I2_131'$  (199.13) [27, 28] (see Fig. 2a). 4-fold and 6-fold double-spin-1 fermions can be found in the B20 material family in the presence of SOC. Materials such as the previously mentioned  $(\text{Rh},\text{Co})(\text{Si},\text{Ge})$  [44],  $\text{AlPt}$  [45],  $\text{PdGa}$  [46] and  $\text{PtGa}$  [47] (see Fig. 2d) are excellent examples of materials hosting these fermions, with extensive theoretical predictions and experimental confirmation of topological properties such as very long Fermi arcs connecting the surface projections of the multifold fermions. 6-fold Dirac fermions have been reported in non-chiral  $\text{PdSb}_2$  [43] (see Fig. 2g and Fig. 2h),  $\text{PtBi}_2$  [48],  $\text{Rb}_4\text{O}_6$  [49],  $\text{Li}_12\text{Mg}_3\text{Si}_4$  [50] and  $\text{SrGePt}$ , which also displays a 4-fold fermion [51].

Finally, 8-fold fermions have also been predicted and found in non-magnetic materials. The 8-fold double-Dirac fermions can exist in seven type II SGs and were predicted in  $\text{Bi}_2\text{AuO}_5$  in MSG  $P4/ncc1'$  (130.424) [52]. Elemental Cs crystals in MSG  $P4_2/mbc1'$  (135.484) also host an 8-fold crossing close to the Fermi level [27, 28] (see Fig. 2b).

#### B. Magnetic materials

Multifolds in magnetic materials are inherently harder to find, due to the relative scarcity of high quality magnetic materials' crystal and magnetic structures reported in the literature.

The most notable example is that of the  $\text{Mn}_3\text{IrSi}$  family ( $\text{Mn}_3\text{IrGe}$ ,  $\text{Mn}_3\text{Ir}_{1-y}\text{Co}_y\text{Si}$ , and  $\text{Mn}_3\text{CoSi}_{1-x}\text{Ge}_x$ ) with type I MSG  $P2_13$  (198.9), which displays a rare example of chiral magnetism. It was predicted to host 3-fold fermions at the R point below the Néel temperature [36] (see Fig. 2c). Above the critical temperature, the magnetic order is destroyed and we recover the full gray group  $P2_131'$  (198.10), in which the 3-folds are forced to

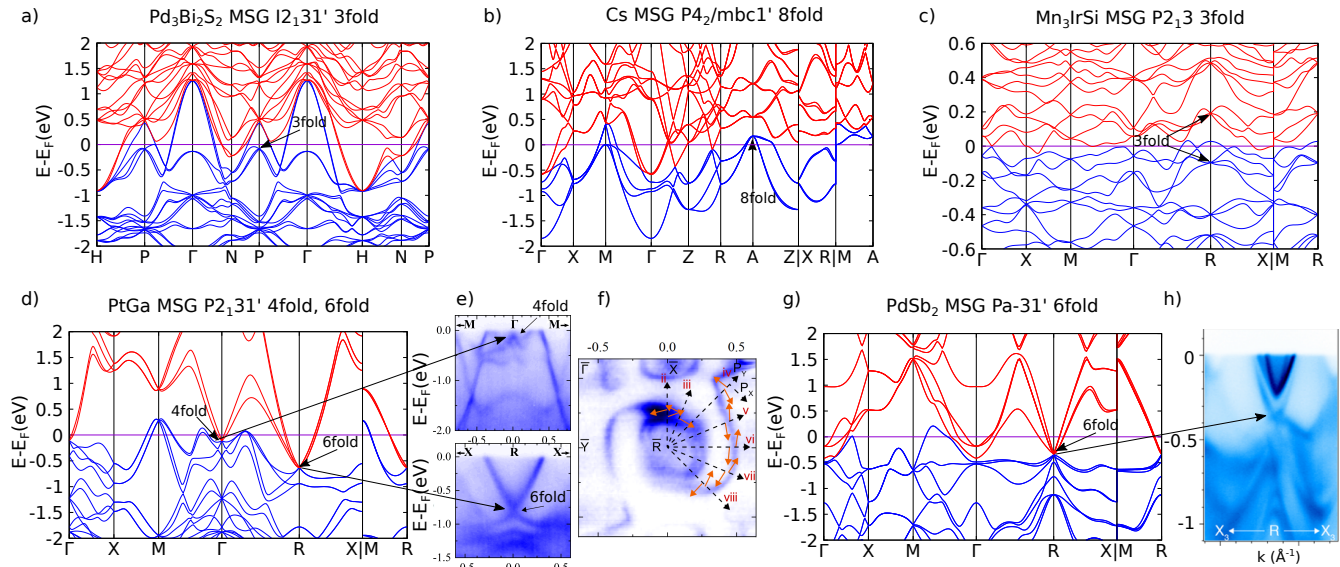


FIG. 2. Crystal structures and electronic bands of non-magnetic and magnetic materials displaying multifold fermions. a)  $\text{Pd}_3\text{Bi}_2\text{S}_2$ , a chiral material displaying a 3-fold fermion at the P point [27, 28]. b) Elemental Cs, in non-Sohnke MSG  $P4_2/\text{mbc}1'$ , displaying an 8-fold fermion close to the Fermi level at A. c)  $\text{Mn}_3\text{IrSi}$  in MSG  $P2_13$  with chiral magnetic ordering displays 3-fold spin-1 fermions at R. d) PtGa in Sohnke MSG  $P2_131'$ , displaying the maximum charge RS 4-fold at  $\Gamma$  and double spin-1 6-fold at R. e) ARPES measurements reported in Ref. [42] showing the bulk band dispersion of both multifold fermions. f) Surface ARPES measurements showing Fermi arcs and their spin polarization. g)  $\text{PdSb}_2$  in non-Sohnke MSG  $\text{Pa-}31'$  presenting a spin-1 Dirac 6-fold fermion at R. h) ARPES measurements reported in Ref. [43] showing the bulk dispersion of the spin-1 Dirac 6-fold (extracted from Ref. [43]). Notice that ARPES measurements for  $\text{PdSb}_2$  were performed at the VUV range [43], while they were performed at the SX range for PtGa [42].

occur in pairs due to TRS.

Following recent advances in the development of high-quality databases for magnetic materials (for instance, MAGNDATA [53]), we are now able to predict several materials in type III MSGs that can host 3-fold fermions, such as  $\text{BaCuTe}_2\text{O}_6$  in MSG  $P4_132'$  (213.65) at the R point [54] and the family of  $\text{La}_3\text{X}_5\text{O}_{12}$  (where La is a lanthanide and  $\text{X}=\text{Ga},\text{Al}$ ) in MSG  $Ia\bar{3}d'$  (230.148) at the P point [55–58]. 6-fold fermions can be found in the TRh ( $\text{T}=\text{Dy}, \text{Ho}, \text{Er}$ ) family of compounds in MSG  $PC2_1/m$  (11.57) [59], as well as in  $\text{Eu}_3\text{PbO}$  with MSG  $P1a\bar{3}$  (205.36) [60], both type IV MSGs. Finally, we predict 8-fold fermions in  $\text{BaNd}_2\text{ZnS}_5$ , with MSG  $PC4/nnc$  (126.385) [61].

### C. Experimental evidence

There are two fundamental experimental signatures of multifold fermions: their bulk band dispersion and Fermi arc surface states. Both can be measured by means of angle-resolved photoemission spectroscopy (ARPES). Due to the short inelastic mean free path photoelectrons in solids of  $\lambda \approx 0.5\text{nm}$  when excited with extreme ultraviolet light (photon energies of  $\approx 10\text{-}150\text{ eV}$ ), this technique has been very successful in imaging topological surface

states [62, 63]. In particular, it has been used to visualize the predicted long Fermi arcs connecting the projection of the 4-fold and 6-fold fermions in the B20 material family [42, 47, 64–66] (see Fig. 2f). These multifold fermions were predicted to carry the maximum topological charge of four, requiring four Fermi arcs to emerge from the surface projection of the multifolds. The four Fermi arcs can be observed in materials where the SOC is large enough to lead to a sizable lifting of the spin-degeneracy, for example, close to the  $\Gamma$  point in PtGa [42] or in PdGa [67]. When SOC is small, it is difficult to resolve the spin-splitting, as in CoSi [66].

To study the bulk electronic structure of solids with ARPES, higher photon energies in the soft X-ray (SX) regime (approx. 150–1500 eV) need to be employed. Here, the inelastic mean free path can typically extend to multiple unit cells, which reduces the effect of momentum broadening in the out of plane direction [68]. Soft X-ray ARPES is therefore more suitable to extract information about the three-dimensional bulk band structure. An example of this can be seen in Fig. 2e, which shows the bulk dispersion of 4-fold and 6-fold multifold fermions in PtGa [42] in ARPES and as predicted by DFT (Fig. 2d), as well as in Fig. 2h, which shows the bulk bands of the 6-fold Dirac in  $\text{PdSb}_2$ . Notice that for the visualization of the sixfold in  $\text{PdSb}_2$  in Fig. 2h, lower photon energies

in the Vacuum-ultraviolet (VUV) range were employed [43].

Even though most of the experimental research has been focused on materials in the B20 family [64, 66, 67, 69–77], PdBiSe, also in MSG P2<sub>1</sub>31' (198.10), exhibits 4-fold and 6-fold fermions which have been experimentally observed [78]. In non-chiral crystals, 6-fold Dirac fermions have been recently found in cubic SG Pa $\bar{3}$ 1' (205.34) in PdSb<sub>2</sub> [43, 79, 80] and in PtBi<sub>2</sub> [48]. Finally, ‘practical’ 8-fold fermions have been reported in TaCo<sub>2</sub>Te<sub>2</sub>[81] in MSG Pnma1' (62.442) without SOC.

#### IV. COMPUTATIONAL METHODS

The calculations presented in Figure 2 have been computed for the purpose of this review based on the structural parameters reported in their respective publications [27, 28, 36, 43, 45]. We performed density functional theory (DFT) calculations as implemented in the Vienna Ab Initio Simulation Package (VASP) [82–85]. The interaction between the ion cores and valence electrons was treated by the projector augmented wave (PAW) method [86], the generalized gradient approximation (GGA) was employed for the exchange-correlation potential with the Perdew–Burke–Ernzerhof for solid parameterization [87] and the SOC was considered on the second variation method [88]. We used a  $\Gamma$ -centered Monkhorst-Pack of  $9 \times 9 \times 9$  k-point grid for reciprocal space integration and we used a 500eV energy cutoff for plane wave expansion. The electronic ground state was self-consistently converged with an accuracy of  $10^{-5}$  eV/unit cell.

#### V. CONCLUSION

This work has reviewed the recent progress in material realizations of multifold fermions from a three-pronged perspective, namely, symmetry arguments, DFT predictions of realistic materials, and experimental realizations. In addition to the basic bulk and surface properties described here, multifold fermions have been predicted to display other interesting physical responses, such as second harmonic generation in B20 RhSi [89], quantized circular photogalvanic effect in multifold fermions [90], non-linear Hall conductivity in CoSi [91] and a new hydrodynamic responses in the B20 family [92]. There has also been research on unconventional superconductivity, with

an unusual s-wave triplet pairing proposed in topological semimetals hosting 3-fold fermions [93]. Finally, the robustness of multifold fermions to disorder is an important question that deserves future study, as Fermi arcs from 3-fold fermions retain their sharpness at weak disorder [94].

With the rapid growth of material predictions in recent years, we expect to see more experimental realizations of these exotic multifold fermions in the future. In particular magnetic systems have recently been the focus of many high-throughput searches [95, 96]. These new materials will prove to be excellent platforms to study multifold fermions and their phenomenology.

#### VI. ACKNOWLEDGEMENTS

M.G.V. and C.F. thank support from the Deutsche Forschungsgemeinschaft (DFG, German Research Foundation) GA3314/1-1 -FOR 5249 (QUAST). M.G.V and I.R. thank support to the Spanish Ministerio de Ciencia e Innovacion grant PID2022-142008NB-I00 and the Ministry for Digital Transformation and of Civil Service of the Spanish Government through the QUANTUM ENIA project call - Quantum Spain project, and by the European Union through the Recovery, Transformation and Resilience Plan - NextGenerationEU within the framework of the Digital Spain 2026 Agenda. This project was partially supported by the European Research Council (ERC) under the European Union’s Horizon 2020 Research and Innovation Programme (Grant Agreement No. 101020833). B.B. acknowledges the support of the Alfred P. Sloan foundation, and the National Science Foundation under grant DMR-1945058. J.C. acknowledges the support of the Alfred P. Sloan foundation, the National Science Foundation under grant DMR-1942447, and the Flatiron Institute, a division of the Simons Foundation. N.B.M.S. was funded by the European Union (ERC Starting Grant ChiralTopMat, project number 101117424). Views and opinions expressed are however those of the author(s) only and do not necessarily reflect those of the European Union or the European Research Council Executive Agency. Neither the European Union nor the granting authority can be held responsible for them. C.F. was financially supported by Deutsche Forschungsgemeinschaft (DFG) under SFB1143 (Project No. 247310070) and Würzburg-Dresden Cluster of Excellence on Complexity and Topology in Quantum Matter—ct.qmat (EXC 2147, project no. 390858490).

---

[1] P. A. M. Dirac. *The Principles of Quantum Mechanics*. Oxford University Press, 4th edition, 1958.  
 [2] H Weyl. GRAVITATION AND THE ELECTRON. *Proc Natl Acad Sci U S A*, 15(4):323–334, April 1929.

[3] Eduardo Fradkin et al. Erratum: Physical realization of the parity anomaly in condensed matter physics [phys. rev. lett. 57, 2967 (1986)]. *Phys. Rev. Lett.*, 58:961–961, Mar 1987.

- [4] Inigo Robredo et al. Higher-order and crystalline topology in a phenomenological tight-binding model of lead telluride. *Phys. Rev. Mater.*, 3:041202, Apr 2019.
- [5] A. H. Castro Neto et al. The electronic properties of graphene. *Rev. Mod. Phys.*, 81:109–162, Jan 2009.
- [6] Zhijun Wang et al. Three-dimensional dirac semimetal and quantum transport in  $\text{cd}_3\text{as}_2$ . *Phys. Rev. B*, 88:125427, Sep 2013.
- [7] Zhijun Wang et al. Dirac semimetal and topological phase transitions in  $\text{A}_3\text{bi}$  ( $a = \text{Na, k, rb}$ ). *Phys. Rev. B*, 85:195320, May 2012.
- [8] Z. K. Liu. A stable three-dimensional topological dirac semimetal  $\text{cd}_3\text{as}_2$ . *Nature Materials*, 13(7):677–681, Jul 2014.
- [9] Z. K. Liu et al. Discovery of a three-dimensional topological dirac semimetal,  $\text{na}_3\text{bi}$ . *Science*, 343(6173):864–867, 2014.
- [10] Conyers Herring. Accidental degeneracy in the energy bands of crystals. *Phys. Rev.*, 52:365–373, Aug 1937.
- [11] Xiangang Wan et al. Topological semimetal and fermi-arc surface states in the electronic structure of pyrochlore iridates. *Phys. Rev. B*, 83:205101, May 2011.
- [12] Kai-Yu Yang et al. Quantum hall effects in a weyl semimetal: Possible application in pyrochlore iridates. *Phys. Rev. B*, 84:075129, Aug 2011.
- [13] A. A. Burkov et al. Weyl semimetal in a topological insulator multilayer. *Phys. Rev. Lett.*, 107:127205, Sep 2011.
- [14] Gang Xu et al. Chern semimetal and the quantized anomalous hall effect in  $\text{hgcr}_2\text{se}_4$ . *Physical review letters*, 107 18:186806, 2011.
- [15] Daniel Bulmash et al. Prediction of a weyl semimetal in  $\text{hg}_{1-x-y}\text{cd}_x\text{mn}_y\text{te}$ . *Phys. Rev. B*, 89:081106, Feb 2014.
- [16] B. Q. Lv et al. Experimental discovery of weyl semimetal  $\text{taas}$ . *Phys. Rev. X*, 5:031013, Jul 2015.
- [17] Su-Yang Xu et al. Discovery of a weyl fermion semimetal and topological fermi arcs. *Science*, 349(6248):613–617, 2015.
- [18] Hongming Weng et al. Weyl semimetal phase in noncentrosymmetric transition-metal monophosphides. *Phys. Rev. X*, 5:011029, Mar 2015.
- [19] Shin-Ming Huang. A weyl fermion semimetal with surface fermi arcs in the transition metal mononictide  $\text{taas}$  class. *Nature Communications*, 6(1):7373, Jun 2015.
- [20] C.J. Bradley et al. *The mathematical theory of symmetry in solids: representation theory for point groups and space groups*. Clarendon Press, 1972.
- [21] J. L. Mañes. Existence of bulk chiral fermions and crystal symmetry. *Phys. Rev. B*, 85:155118, Apr 2012.
- [22] S. M. Young et al. Dirac semimetal in three dimensions. *Phys. Rev. Lett.*, 108:140405, Apr 2012.
- [23] Julia A. Steinberg et al. Bulk dirac points in distorted spinels. *Phys. Rev. Lett.*, 112:036403, Jan 2014.
- [24] Benjamin J. Wieder et al. Spin-orbit semimetals in the layer groups. *Phys. Rev. B*, 94:155108, Oct 2016.
- [25] Barry Bradlyn, Jennifer Cano, Zhijun Wang, M. G. Vergniory, C. Felser, R. J. Cava, and B. Andrei Bernevig. Beyond dirac and weyl fermions: Unconventional quasiparticles in conventional crystals. *Science*, 353(6299):aaf5037, 2016.
- [26] Benjamin J. Wieder et al. Double dirac semimetals in three dimensions. *Phys. Rev. Lett.*, 116:186402, May 2016.
- [27] M. G. Vergniory. A complete catalogue of high-quality topological materials. *Nature*, 566(7745):480–485, Feb 2019.
- [28] Maia G. Vergniory et al. All topological bands of all nonmagnetic stoichiometric materials. *Science*, 376(6595):eabg9094, 2022.
- [29] Tiantian Zhang. Catalogue of topological electronic materials. *Nature*, 566(7745):475–479, Feb 2019.
- [30] Feng Tang. Comprehensive search for topological materials using symmetry indicators. *Nature*, 566(7745):486–489, Feb 2019.
- [31] J. Perez-Mato et al. Crystallography online: Bilbao crystallographic server. *Bulgarian Chemical Communications*, 43:183–197, 01 2011.
- [32] M. Ilia et al. Bilbao crystallographic server: I. databases and crystallographic computing programs. *Zeitschrift für Kristallographie - Crystalline Materials*, 221(1):15–27, 2006.
- [33] M. Ilia et al. Bilbao Crystallographic Server. II. Representations of crystallographic point groups and space groups. *Acta Crystallographica Section A*, 62(2):115–128, Mar 2006.
- [34] Barry Bradlyn et al. Beyond dirac and weyl fermions: Unconventional quasiparticles in conventional crystals. *Science*, 353:6299, 2016.
- [35] Guoqing Chang et al. Topological quantum properties of chiral crystals. *Nature materials*, 17(11):978–985, 2018.
- [36] Jennifer Cano et al. Multifold nodal points in magnetic materials. *APL Materials*, 7(10):101125, 2019.
- [37] Technically, the RS fermion Hamiltonian is not analytic in  $k$  (Eq. (7) in Ref. [36]) because the second term contains  $k^2$  in the denominator. The authors decided to re-name only the analytic part as  $\text{RS}^*$  fermion, which is the Hamiltonian of the form  $H_{3/2} = \mathbf{k} \cdot \mathbf{S}^{3/2}$  with  $S_{x,y,z}^{3/2}$  the generators of the spin  $s = 3/2$  representation.
- [38] Long Liang et al. Semimetal with both rarita-schwinger-weyl and weyl excitations. *Phys. Rev. B*, 93:045113, Jan 2016.
- [39] Peizhe Tang et al. Multiple types of topological fermions in transition metal silicides. *Phys. Rev. Lett.*, 119:206402, Nov 2017.
- [40] Kirill Alpin et al. Fundamental laws of chiral band crossings: Local constraints, global constraints, and topological phase diagrams. *Phys. Rev. Res.*, 5:043165, Nov 2023.
- [41] Barry Bradlyn et al. Topological quantum chemistry. *Nature*, 547:298–305, 2017.
- [42] Jonas A. Krieger et al. Parallel spin-momentum locking in a chiral topological semimetal, 2022.
- [43] Nitesh Kumar et al. Signatures of sixfold degenerate exotic fermions in a superconducting metal  $\text{pdsb}_2$ . *Advanced Materials*, 32(11):1906046, 2020.
- [44] Peizhe Tang et al. Multiple types of topological fermions in transition metal silicides. *Phys. Rev. Lett.*, 119:206402, Nov 2017.
- [45] N. Schroeter et al. Chiral topological semimetal with multifold band crossings and long fermi arcs. *Nature Physics*, 15(8):759–765, Aug 2019.
- [46] Paolo Sessi. Handedness-dependent quasiparticle interference in the two enantiomers of the topological chiral semimetal  $\text{pdga}$ . *Nature Communications*, 11(1):3507, Jul 2020.
- [47] Mengyu Yao. Observation of giant spin-split fermi-arc with maximal chern number in the chiral topological



- semimetal ptga. *Nature Communications*, 11(1):2033, Apr 2020.
- [48] S. Thirupathaiyah et al. Sixfold fermion near the Fermi level in cubic PtBi2. *SciPost Phys.*, 10:004, 2021.
- [49] Lei Jin et al. Spin-polarized sextuple excitations in ferromagnetic materials. *Phys. Rev. B*, 105:245141, Jun 2022.
- [50] Simin Nie et al. Sixfold excitations in electrides. *Phys. Rev. Res.*, 3:L012028, Mar 2021.
- [51] Yi Shen et al. Chiral topological metals with multiple types of quasiparticle fermions and large spin hall effect in the srgept family materials. *Phys. Rev. B*, 108:035428, Jul 2023.
- [52] Benjamin J. Wieder et al. Double dirac semimetals in three dimensions. *Phys. Rev. Lett.*, 116:186402, May 2016.
- [53] S. Gallego et al. MAGNDATA: towards a database of magnetic structures. I.The commensurate case. *Journal of Applied Crystallography*, 49(5):1750–1776, Oct 2016.
- [54] A. Samartzis et al. Structural and magnetic properties of the quantum magnet  $\text{BaCu}_2\text{O}_6$ . *Phys. Rev. B*, 103:094417, Mar 2021.
- [55] J. Hammann. Etude par diffraction de neutrons à  $0,31^\circ\text{K}$  de la structure antiferromagnétique des grenats d'aluminium-terbium et d'aluminium-holmium. *Acta Crystallographica Section B*, 25(9):1853–1856, Sep 1969.
- [56] Wawrzyniak. Magnetic order and single-ion anisotropy in  $\text{tb}_3\text{ga}_5\text{o}_{12}$ . *Phys. Rev. B*, 100:094442, Sep 2019.
- [57] Y. Cai et al. Crystal fields and magnetic structure of the ising antiferromagnet  $\text{er}_3\text{ga}_5\text{o}_{12}$ . *Phys. Rev. B*, 100:184415, Nov 2019.
- [58] I. A. Kibalin et al. Competing interactions in dysprosium garnets and generalized magnetic phase diagram of  $S = \frac{1}{2}$  spins on a hyperkagome network. *Phys. Rev. Res.*, 2:033509, Sep 2020.
- [59] van Nhung. Structures magnetiques des composés equiatomiques terres rares-rhodium  $\text{trh}(t = \text{dy, ho, er})$ . *Solid State Communications*, 10(8):685–689, 1972.
- [60] Moritz M. Hirschmann et al. Creating and controlling dirac fermions, weyl fermions, and nodal lines in the magnetic antiperovskite  $\text{eu}_3\text{PbO}$ . *Phys. Rev. Mater.*, 6:114202, Nov 2022.
- [61] Madalynn Marshall. Field-induced partial disorder in a shastry-sutherland lattice. *Nature Communications*, 14(1):3641, Jun 2023.
- [62] Haifeng Yang. Visualizing electronic structures of quantum materials by angle-resolved photoemission spectroscopy. *Nature Reviews Materials*, 3(9):341–353, Sep 2018.
- [63] Baiqing Lv. Angle-resolved photoemission spectroscopy and its application to topological materials. *Nature Reviews Physics*, 1(10):609–626, Oct 2019.
- [64] Daniel S. Sanchez. Topological chiral crystals with helicoid-arc quantum states. *Nature*, 567(7749):500–505, Mar 2019.
- [65] Guoqing Chang et al. Unconventional chiral fermions and large topological fermi arcs in rhsi. *Phys. Rev. Lett.*, 119:206401, Nov 2017.
- [66] Daichi Takane et al. Observation of chiral fermions with a large topological charge and associated fermi-arc surface states in cosi. *Phys. Rev. Lett.*, 122:076402, Feb 2019.
- [67] Niels B. M. Schröter et al. Observation and control of maximal chern numbers in a chiral topological semimetal. *Science*, 369(6500):179–183, 2020.
- [68] VN Strocov. Intrinsic accuracy in 3-dimensional photoemission band mapping. *Journal of Electron Spectroscopy and related phenomena*, 130(1-3):65–78, 2003.
- [69] Hang Li. Chiral fermion reversal in chiral crystals. *Nature Communications*, 10(1):5505, Dec 2019.
- [70] Zhicheng Rao. Observation of unconventional chiral fermions with long fermi arcs in cosi. *Nature*, 567(7749):496–499, Mar 2019.
- [71] Zhicheng Rao et al. Charge instability of topological fermi arcs in chiral crystal cosi, 2021.
- [72] Bing Xu et al. Optical signatures of multifold fermions in the chiral topological semimetal cosi. *Proceedings of the National Academy of Sciences*, 117:27104–27110, 2020.
- [73] Xitong Xu et al. Crystal growth and quantum oscillations in the topological chiral semimetal cosi. *Phys. Rev. B*, 100:045104, Jul 2019.
- [74] Qian-Qian Yuan et al. Quasiparticle interference evidence of the topological fermi arc states in chiral fermionic semimetal cosi. *Science Advances*, 5(12):eaaw9485, 2019.
- [75] S. Changdar et al. Electronic structure studies of fes: A chiral topological system. *Phys. Rev. B*, 101:235105, Jun 2020.
- [76] Tyler A. Cochran et al. A fermi arc quantum ladder, 2020.
- [77] Daniel S. Sanchez. Tunable topologically driven fermi arc van hove singularities. *Nature Physics*, 19(5):682–688, May 2023.
- [78] B. Q. Lv et al. Observation of multiple types of topological fermions in pdbise. *Phys. Rev. B*, 99:241104, Jun 2019.
- [79] Xián Yáng et al. Observation of sixfold degenerate fermions in  $\text{PdSb}_2$ . *Phys. Rev. B*, 101:201105, May 2020.
- [80] Woori Ju et al. Fine details of sixfold dirac fermions in pyrite-structured  $\text{pdsb}_2$ . *Phys. Rev. B*, 106:205125, Nov 2022.
- [81] Hongtao Rong. Realization of practical eightfold fermions and fourfold van hove singularity in  $\text{taco2te}_2$ . *npj Quantum Materials*, 8(1):29, May 2023.
- [82] G. Kresse et al. Ab initio molecular dynamics for liquid metals. *Phys. Rev. B*, 47:558–561, Jan 1993.
- [83] G. Kresse et al. Ab initio molecular-dynamics simulation of the liquid-metal-amorphous-semiconductor transition in germanium. *Phys. Rev. B*, 49:14251–14269, May 1994.
- [84] G. Kresse et al. Efficiency of ab-initio total energy calculations for metals and semiconductors using a plane-wave basis set. *Computational Materials Science*, 6(1):15–50, 1996.
- [85] G. Kresse et al. Efficient iterative schemes for ab initio total-energy calculations using a plane-wave basis set. *Phys. Rev. B*, 54:11169–11186, Oct 1996.
- [86] P. E. Blöchl. Projector augmented-wave method. *Phys. Rev. B*, 50:17953–17979, Dec 1994.
- [87] John P. Perdew et al. Generalized gradient approximation made simple. *Phys. Rev. Lett.*, 77:3865–3868, Oct 1996.
- [88] Soner Steiner et al. Calculation of the magnetic anisotropy with projected-augmented-wave methodology and the case study of disordered  $\text{fe}(1-x)\text{cox}$  alloys. *Phys. Rev. B*, 93:224425, Jun 2016.
- [89] Baozhu Lu et al. Second-harmonic generation in the topological multifold semimetal rhsi. *Phys. Rev. Res.*, 4:L022022, Apr 2022.



- [90] Felix Flicker et al. Chiral optical response of multifold fermions. *Phys. Rev. B*, 98:155145, Oct 2018.
- [91] V. D. Esin. Nonlinear planar hall effect in chiral topological semimetal *cosi*. *Journal of Experimental and Theoretical Physics*, 133(6):792–797, Dec 2021.
- [92] Iñigo Robredo et al. Cubic hall viscosity in three-dimensional topological semimetals. *Phys. Rev. Res.*, 3:L032068, Sep 2021.
- [93] GiBaik Sim. Topological triplet-superconductivity in spin-1 semimetal. *Communications Physics*, 5(1):220, Sep 2022.
- [94] Hsiu-Chuan Hsu et al. Disorder effects on triple-point fermions. *Phys. Rev. B*, 106:245118, Dec 2022.
- [95] Yuanfeng Xu. High-throughput calculations of magnetic topological materials. *Nature*, 586(7831):702–707, Oct 2020.
- [96] Yunlong Su. High-throughput first-principle prediction of collinear magnetic topological materials. *npj Computational Materials*, 8(1):261, Dec 2022.